ELSEVIER

Journal of Crystal Growth 220(2000) 166–175

JOURNAL OF CRYSTAL GROWTH

www.elsevier.nl/locate/jcrysgro

Analysis of the unsteady segregation in crystal growth from a melt
Part II: Fluctuating convection velocity

F.Z. Haddad[a,*], J.P. Garandet[b], D. Henry[a], H. Ben Hadid[a]

[a]*Laboratoire de Mécanique des Fluides et d'Acoustique, Ecole Centrale de Lyon/UCB Lyon 1, UMR CNRS 5509, ECL, BP 163, 69131 Ecully Cedex, France*

[b]*Commissariat à l'Energie Atomique, DTA/CEREM/DEM/SPCM/LRBS, CEA Grenoble, 17 rue des martyrs, 38054 Grenoble Cedex 9, France*

Received 5 November 1999; accepted 26 June 2000
Communicated by D.T.J. Hurle

Abstract

The purpose of this paper is to analyse the correlations between convection fluctuations and segregation in the crystal during solidification in the horizontal Bridgman configuration. The effects of both the amplitude and the frequency of the convection velocity oscillations on the axial and radial segregation will be determined. The results will be compared with predictions based on an analytical model.

Keywords: Segregation; Bridgman; Instationarity

1. Introduction

It is now well accepted that the study of transport phenomena in the melt is important for the optimisation of solidification processes. In crystal growth from the melt, the influence of steady convective motions on segregation is clearly identified (see e.g. Ref. [1–4]). Comparatively little attention has been paid to unsteady convection, that is known to lead to detrimental composition striations in alloys [5]. In a companion paper [6], we investigated numerically the effect of fluctuations of the growth velocity on segregation, and our present purpose is to extend our previous work to the problem of oscillating convection velocities.

Unsteady convection in the melt may act directly on the solute field, as in the case of *g*-jitters in microgravity solidification [7], but also indirectly via the induced variations of the growth rate if the coupling with heat transport is strong enough. The topic has been approached by Jung and Müller [8], using a full numerical modeling of the heat, momentum and mass transport phenomena. Interesting results were thus obtained, but, due to the complexity of the problem, the detailed mechanisms of transient solute incorporation were not fully elucidated.

In the present work, we shall only focus on the direct effect of unsteady convection, since we consider the Prandtl number of the model material to

* Corresponding author. Fax: + 33-4-7864-7145.
E-mail address: haddad@mecaflu.ec-lyon.fr (F.Z. Haddad).

0022-0248/00/$ - see front matter
PII: S0022-0248(00)00587-X

Nomenclature

A	aspect radio of the cavity ($A = L/H$)
C	solute composition in the melt (mass fraction)
C_0	initial solute composition in the melt
C^0	time independent part of C
C_I^0	C^0 at the interface
C^1	amplitude of the time fluctuation of C
C_I^1	C^1 at the interface
C_l	longitudinal segregation
C_n	normalized longitudinal segregation
$\lvert C_\mathrm{n}\rvert$	peak-to-peak amplitude of the oscillations of C_n
$C_{\mathrm{n}'}$	normalized radial segregation
$\lvert C_{\mathrm{n}'}\rvert$	peak-to-peak amplitude of the oscillations of $C_{\mathrm{n}'}$
C_r	radial segregation
c	non-dimensional solute composition in the melt
c_s	non-dimensional solute composition in the crystal
D	solute diffusion coefficient ($\mathrm{m^2\,s^{-1}}$)
G_S	static gain of the low pass filter
g	gravity ($\mathrm{m\,s^{-2}}$)
H	height of the cavity (m)
j	complex number
k	solute equilibrium partition ratio of the binary alloy ($k = 0.087$)
L	length of the cavity (m)
l	filter order
S	non-dimensional length of the melt zone
T	non-dimensional oscillation peirod
T_C	non-dimensional cut-off period
t	non-dimensional time
t_d	time (s)
u	non-dimensional horizontal convective velocity component
V_c	convection velocity ($\mathrm{m\,s^{-1}}$)
v_c	non-dimensional convection velocity
$v_{\mathrm{c},s}$	non-dimensional constructed convective flow for a melt zone of length S
$\overline{V_\mathrm{c}}(\delta)$	space averaged convection velocity in the frame of the solutal 1D boundary layer model
V_c^0	time independent part of $\lvert\overline{V_\mathrm{c}}(\delta)\rvert$
V_c^1	amplitude of the time fluctuation of $\lvert\overline{V_\mathrm{c}}(\delta)\rvert$
V_eff	effective transport velocity ($\mathrm{m\,s^{-1}}$)
V_I	interface velocity ($\mathrm{m\,s^{-1}}$)
v_I	non-dimensional interface velocity
ω	non-dimensional vertical convective velocity component
X	horizontal coordinate
x	non-dimensional horizontal coordiante
z	non-dimensional vertical coordinate
Gr	Grashof number, $\mathrm{Gr} = g\beta H^4\nabla\theta/\nu^2$
Pe	Péclet number, $\mathrm{Pe} = -HV_\mathrm{I}/D$
Pr	Prandtl number, $\mathrm{Pr} = \nu/\kappa$
Sc	Schmidt number, $\mathrm{Sc} = \nu/D$

Greek letters

α	relative amplitude of the convective velocity osillation
β	thermal expansion coefficient
Δ	convecto diffusive parameter ($0 \leqslant \Delta \leqslant 1$)
δ	solute boundary layer thickness (m)
κ	thermal diffusivity of the melt ($\mathrm{m^2\,s^{-1}}$)
∇	nabla operator
$\nabla\theta$	applied thermal gradient in the cavity
ν	kinematic viscosity of the melt ($\mathrm{m^2\,s^{-1}}$)
Ω	non-dimensional pulsation ($\Omega = \omega\delta^2/D$)
Ω_C	non-dimensional cut-off pulsation
ω	pulsation of the perturbation ($\mathrm{s^{-1}}$)
ω_C	cut-off pulsation of the perturbation ($\mathrm{s^{-1}}$)
π	pi number

be strictly equal to zero, which means that heat transport is not affected by the velocity. Our formulation is thus much simpler than Jung and Müller's, since we assume the oscillating convection velocity to be a given input in the solute conservation equation. Our purpose is to characterize the axial and radial solute segregations induced by such an oscillating velocity in a model horizontal Bridgman configuration. The imposed fluctuations will cover a large amplitude and frequency range to allow

comparison of the numerical results with the predictions of an existing analytical model.

As done in our previous work [6], we shall first recall in Section 2 the main features of a simplified analytical model accounting for the effect of unsteady convection velocity on composition. Then, in Section 3, the physical model and the numerical procedure are briefly presented. Section 4 is dedicated to the analysis of the simulation results. A discussion of the accuracy of the analytical model, and of its ability to capture the physics of solute transport phenomena both in quasi-steady and transient problems, is also carried out.

2. Outline of the analytical solution

Our purpose in this section is to briefly recall the main features of an analytical model that allows to derive the composition response to a given convection velocity perturbation, since it will be thoroughly used in the following for comparison with the numerical results. For more details on the starting assumptions and the procedure, the interested reader is referred to the original publications [9,10]. To start with, let us consider the time-dependent mass conservation equation, written in a reference frame moving with the interface:

$$\partial C/\partial t_d + (\boldsymbol{V}_c \cdot \nabla)C = D\nabla^2 C + (\boldsymbol{V}_I \cdot \nabla)C. \quad (1)$$

In the above equation, C, D, $\boldsymbol{V}_c$, $\boldsymbol{V}_I$, and t_d respectively stand for solute concentration, diffusion coefficient, convection velocity, growth rate, and time. A first assumption is to drop the radial composition derivatives, that is to suppose that the concentration variations take place principally along the normal to the interface, X in the notations of the present paper. However, the key idea is to account for convective effects in the frame of the solutal boundary layer model [11] through $\overline{V_c}(\delta)$, mean convective velocity evaluated at $X = \delta$ ($\overline{V_c}(\delta) \geqslant 0$ and $V_I \leqslant 0$ in the notations of the present paper, see the reference frame in Fig. 1), which yields

$$\partial C/\partial t_d = D\partial^2 C/\partial X^2 + V_{eff}\partial C/\partial X, \quad (2)$$

with $V_{eff} = \overline{V_c}(\delta) - V_I$. The effective transport velocity V_{eff} can be related to the solutal boundary layer thickness δ of the associated steady-state problem through $V_{eff} = D/\delta$ [11]. This allows to define the convecto-diffusive parameter Δ as $|V_I|/V_{eff}$ or $|V_I|\delta/D$; Δ, which corresponds to a normalized boundary layer thickness, was found to be a relevant measure of the influence of convection on mass transfer [4,11]. Then, in line with an approach originally proposed by Hurle et al. [12], a solution to Eq. (2) is obtained through a Fourier series expansion up to the order 1 of the main variables of the problem. For instance, the form of the composition field is given as

$$C(X, t_d) = C^0(X) + C^1(X)\exp(j\omega t_d). \quad (3)$$

The convection velocity fluctuation V_c^1 ($\overline{V_c}(\delta) = V_c^0 + V_c^1\exp(j\omega t_d)$ with $V_c^0 \geqslant 0$ and $V_c^1 \geqslant 0$) is assumed small enough to neglect the second-order term $V_c^1 C^1$ in Eq. (2). Even with these assumptions, the algebra involved is fairly tedious, and the interested reader is referred to the original publications

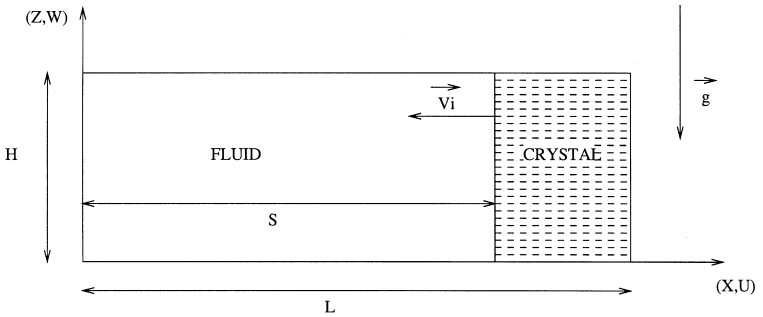

Fig. 1. Studied configuration.

for details on the derivation. However, for our present purposes, a composite solution can be built based on the asymptotic high frequency and low-frequency regimes [9,10]. The relation between normalized convection velocity and interface composition fluctuations can be expressed as

$$C_I^1/C_I^0 = [G_S/(1 + j\Omega/\Omega_C)]V_c^1/V_c^0, \quad (4)$$

where the pulsation Ω is defined as $\Omega = \omega\delta^2/D$. The variables G_S and Ω_C, respectively, stand for the static gain and the cut-off pulsation of this first-order linear filter and j is the complex number such that $j^2 = -1$. Numerically, G_S and Ω_C are given as

$$G_S = -(1-k)\Delta(1-\Delta)/[1-(1-k)\Delta], \quad (5)$$

$$\Omega_C = 1-(1-k)\Delta. \quad (6)$$

From a physical standpoint, the minus sign in the expression of G_S indicates that an increase of the convection level induces a decrease in terms of interfacial composition. Moreover as noted in Ref. [12], the occurrence of imaginary terms in relation (4) is related to a phase shift between the convection velocity and interface composition fluctuations. It should be noted that the Δ featured in expressions (5) and (6) should be deduced from the analysis of axial composition profiles based on the mean convection velocity. It is not in any case a free parameter. In that respect, our present work is also a new test of the capacity of the boundary layer model to capture the physics of transient segregation phenomena.

3. Physical model and numerical procedure

Let us recall the basic points of our numerical modeling. We invite the interested reader to refer to Section 3 of Ref. [6] in which we explain the mathematical model in more detail. The physical system schematically represented in Fig. 1, represents a rectangular cavity filled with a strictly equal zero Prandtl number diluted alloy. The solid–liquid interface is supposed to be planar and to move at a constant velocity V_I. Convection in the melt is driven by thermal buoyancy force and the concentration field is assumed to have no feedback on the flow field so that it can be studied separately. In the following, mainly non-dimensional variables will be used: practically, length, velocity, time, and concentration have been respectively normalized by H, v/H, H^2/v, and C_0 (initial solute concentration in the melt).

To simulate a solidification process by the horizontal Bridgman technique with an oscillatory convection velocity, one possibility is to take a sufficiently high Grashof number, for which the flow becomes naturally oscillatory. In fact, for the cavity of aspect ratio $A = L/H = 4$ that we have chosen, this flow corresponds to three oscillatory rolls [13]; however, the reduction of the size of the liquid zone during solidification not only will modify the structure of the flow, but also will stabilize the oscillations, which makes difficult any interpretation. We then chose a more academic case where the oscillations of convection are regular. We used the fact that at first approximation, for a fluid with Grashof number not too high, the convection in a lengthened cell presents a central zone with an almost parallel and uniform flow and end zones of length equal to the height for the reversal of the flow [13] (see Fig. 2). We have chosen to compute the unicellular steady flow for $Gr = 5000$ ($Pr = 0$) for a cavity of aspect ratio $A = 2$, and from it we have constructed the steady flow $v_{c,S}(x,z)$ for a liquid zone of length $S > 2$ by adding a central zone with parallel and uniform flow. This steady flow nearly corresponds to the real flow at $Gr = 5000$, although the real flow is not so perfectly parallel in the central zone and is a little more convective, because it is less confined, particularly at the beginning of solidification. The non-dimensional oscillatory velocity used in the simulations can thus be written as

$$v_c(x,z,t) = v_{c,S}(x,z)\left(1 + \alpha\sin\left(\frac{2\pi t}{T}\right)\right) \quad (7)$$

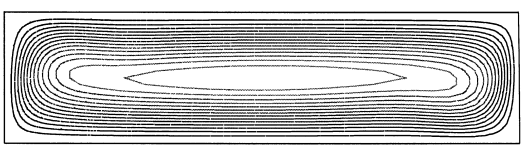

Fig. 2. Fluid flow represented by streamlines for $A = 4$ and $Gr = 5000$.

with $\alpha > 0$. α and T stand respectively for the relative amplitude and the non-dimensional period of the velocity perturbations.

The convective field being thus imposed, we will have only the mass transport equation to solve in the liquid phase, and the segregation in the solid phase will be deduced by the relation

$$c_s = kc,$$

where c_s and c are respectively the concentrations in the solid and liquid phases and k is the equilibrium partition ratio. In its non-dimensional form and in a fixed domain of calculation, the mass transport equation is written as (see Ref. [3])

$$\frac{\partial c}{\partial t} + (u - xv_I)\frac{1}{S}\frac{\partial c}{\partial x} + w\frac{\partial c}{\partial z} = \frac{1}{\mathrm{Sc}}\left[\frac{1}{S^2}\frac{\partial^2 c}{\partial x^2} + \frac{\partial^2 c}{\partial z^2}\right],$$

where v_I is the non-dimensional interface velocity, u and w the components of the imposed convective field $v_c(x, z, t)$, and Sc the Schmidt number. The boundary equation expressing the condition of mass conservation at the solid–liquid interface is written as

$$\frac{\partial c}{\partial x} = \mathrm{Pe}(1 - k)c,$$

where Pe is the Péclet number. The other boundaries are supposed to be solid and impermeable. In the following calculations the Schmidt and Péclet numbers are fixed (Sc = 10 and Pe = 2). The mesh used is generated by Thompson's technique [14]. The nodes are squeezed near the walls of the cavity and specially in the vicinity of the solid–liquid interface because of high-composition gradients there. The problem is solved by using a Hermitian finite difference method with an alternative implicit direction scheme [15] in a grid of 25×101 points on (z, x) directions, which proved to give sufficiently accurate results for such studies [3]. In our numerical computations, a cavity of aspect ratio $A = 4$ is used and the solidification was conducted over the first half of the cavity. We shall focus on two quantities: the amplitude of the normalized segregation oscillations and their phase shift with respect to the imposed oscillatory convection velocity.

4. Results and discussion

We want to analyse the longitudinal and radial segregations (C_l and C_r) which are defined respectively as the mean value of the concentration in the solid, c_s, along the interface and the normalized maximum difference of c_s along the interface:

$$C_l = \int_0^1 c_s(z, S)\,\mathrm{d}z$$

$$C_r = \frac{c_{s,\max}(S) - c_{s,\min}(S)}{C_l}.$$

In Figs. 3(a) and (b) we give the evolutions of respectively the longitudinal and the radial segregation for a case of an oscillatory convection velocity v_c with $\alpha = 0.5$ and $T = 0.5$ along with those obtained in the case of a nonoscillatory convection

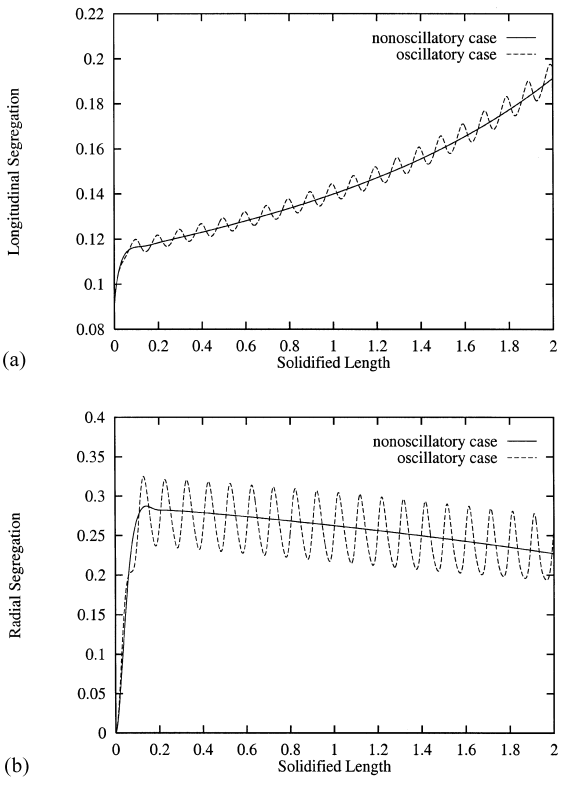

Fig. 3. Segregation responses for steady and unsteady ($\alpha = 0.5, T = 0.5$) cases: (a) longitudinal segregations, (b) radial segregations.

velocity $v_{c,S}$. We notice that the oscillations of the segregation for the unsteady case fluctuate on both sides of the segregation profile for the steady case. As done in our previous work [6], for a better characterization of the oscillatory signals of segregation, we define the normalized longitudinal segregation C_n and the normalized radial segregation $C_{n'}$ as

$$C_n = \frac{C_{l,v} - C_{l,c}}{C_{l,c}}$$

$$C_{n'} = C_{r,v} - C_{r,c},$$

the indices v and c referring respectively to the variable and constant velocity cases. The evolution of the normalized segregations corresponding to the case of Fig. 3 are given in Fig. 4.

Let us recall that, as done previously [3,6], the convecto-diffusive parameter Δ is deduced from a best fit of the longitudinal segregation profiles according to Favier's model [16].

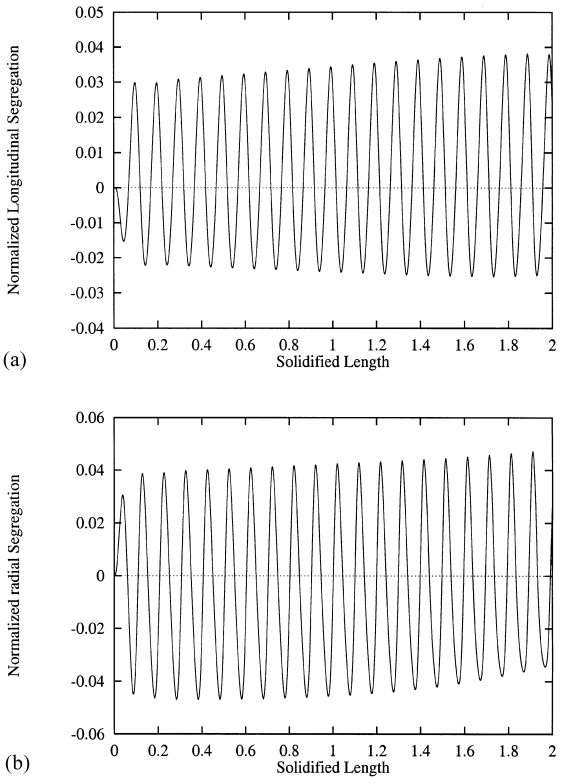

Fig. 4. Normalized segregations ($\alpha = 0.5, T = 0.5$): (a) normalized longitudinal segregation, (b) normalized radial segregation.

4.1. Longitudinal segregation

It should be remembered that the amount of incorporated solute decreases when the convection increases, with, for the convective mode to which $Gr = 5000$ belongs, a characteristic variation of the convecto-diffusive parameter Δ in $(Gr\,Sc)^{-1/3}$ [17] and a linear dependence of C_l on Δ. If we consider the case $\alpha = 0.5$, the variation of the convection is equivalent to a variation of Gr between 2500 and 7500. The first oscillatory velocity variation is positive what explains the initial decrease of the segregation. In addition, the nonlinear variation according to Gr (in power $-1/3$) explains the difference in amplitudes between the positive and the negative oscillations of the normalized segregation. Indeed, the ratio between these amplitudes, as obtained from the characteristic relationship for Δ, is about

$$\frac{(2500^{-1/3} - 5000^{-1/3})/5000^{-1/3}}{(5000^{-1/3} - 7500^{-1/3})/5000^{-1/3}} \sim \frac{0.01519}{0.0074} \sim 2.05,$$

which is a rough estimation of the observed ratio between positive and negative oscillation amplitudes in Fig. 4(a).

As opposed to our previous work on interface velocity fluctuations [6], the amplitude of the composition oscillations is not perfectly constant along solidification. We used as a measure of the effect of the fluctuating convection level the average of the peak-to-peak amplitudes, denoted $|C_n|$, over the first half of the crystal, the initial transitory stage being excluded. Concerning the phase shift ϕ, it is also not perfectly constant along solidification, and so a similar averaging procedure is used. Moreover, different values are found if the estimation is made on the maxima or minima of the concentration variations, which necessitates to take a mean value between both estimations. This last observation can be connected to the fact that the maxima and minima of concentration correspond respectively to minima and maxima of flow velocity for which the boundary layer thickness is different. Then the time for the perturbation to go from the bulk flow to the solidification interface will also be different. The same procedures will be used for the estimation

of amplitudes $|C_{n'}|$ and phase shifts for the radial segregation.

4.1.1. Effect of the perturbation amplitude

The evolution of the amplitude $|C_n|$ according to α for the period $T = 0.5$ shows a linear behavior for the small values of α, the system leaving the linearity domain beyond $\alpha = 0.5$ (Fig. 5(a)).

Fig. 5(b) giving the phase shift ϕ between $v_c(x, z, t)$ and C_n according to α shows that the delay of the response of C_n to the velocity excitation $v_c(x, z, t)$ is almost constant, around 0.35π.

4.1.2. Effect of the perturbation period

The evolution of $|C_n|$ according to T for the amplitude $\alpha = 0.2$ exhibits an increase for small periods (large frequencies) and an asymptotic constant regime for large periods, the cut-off period being located around $T = 0.4$ (Fig. 6(a)).

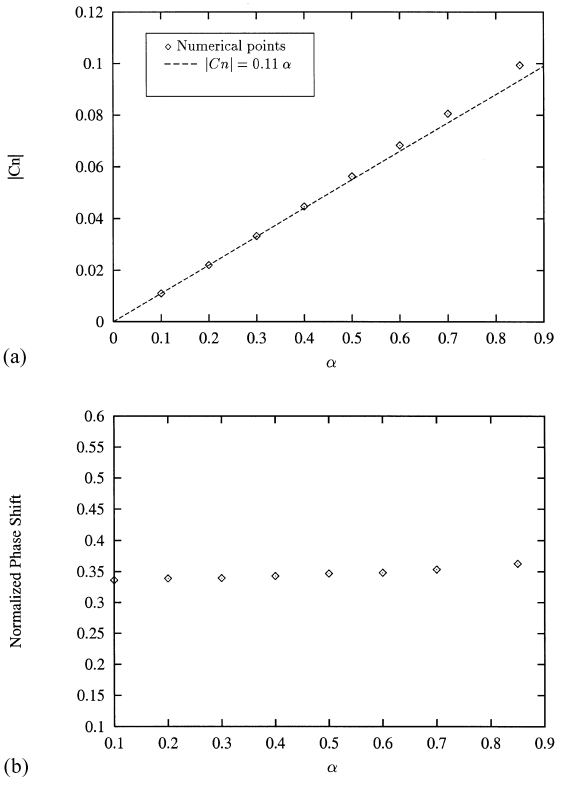

Fig. 5. Amplitude and phase shift of C_n ($T = 0.5$): (a) variation of the amplitude $|C_n|$ with α, (b) phase shift $\phi(v_c, C_n)/\pi$ as a function of α.

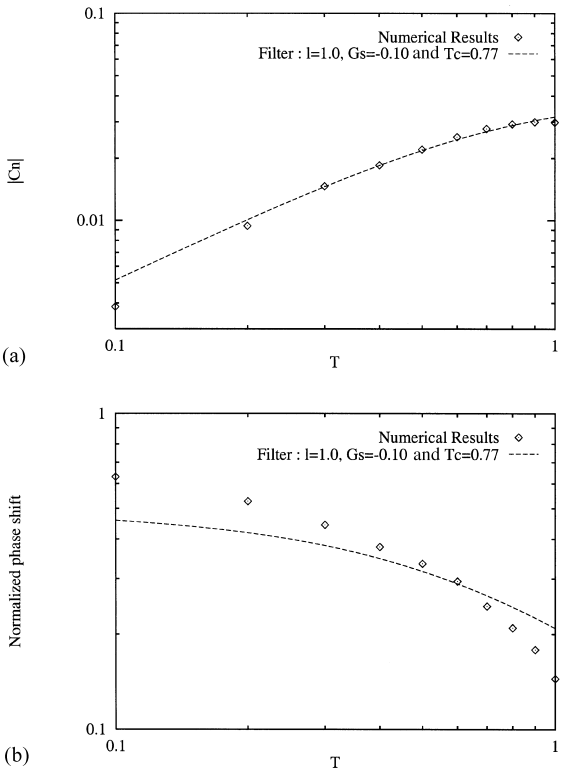

Fig. 6. Amplitude and phase shift of C_n ($\alpha = 0.2$): (a) variation of the amplitude $|C_n|$ with T, (b) phase shift $\phi(v_c, C_n)/\pi$ as a function of T.

As for the phase shift between the oscillatory velocity signal and the oscillatory segregation response, Fig. 6(b) shows that this delay is about 0.63π for the period $T = 0.1$ and that it decreases when T increases. For large periods, the longitudinal segregation follows almost instantaneously the convective velocity excitation.

It can be checked that all these features compare favorably with those predicted by the analytical model presented in Section 2 (Eq. (4)). A more detailed comparison between numerical and analytical results will be presented in Section 4.4.

4.2. Radial segregation

4.2.1. Effect of the perturbation amplitude

In Fig. 7(a) we plot the curve of evolution of the amplitude $|C_{n'}|$ according to α for the case $T = 0.5$. We notice again a linearity of this evolution for the

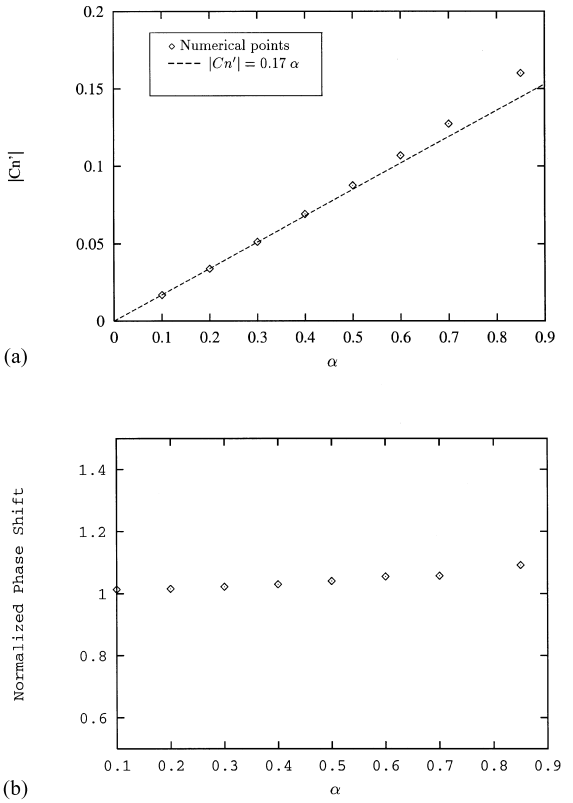

Fig. 7. Amplitude and phase shift of $C_{n'}(T = 0.5)$: (a) variation of the amplitude $|C_{n'}|$ with α, (b) phase shift $\phi(v_c, C_{n'})/\pi$ as a function of α.

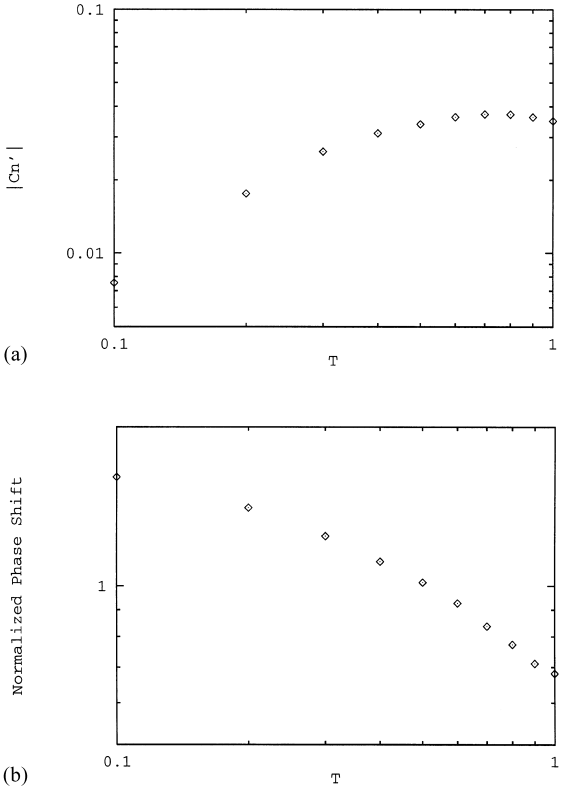

Fig. 8. Amplitude and phase shift of $C_{n'}$ ($\alpha = 0.2$): (a) variation of the amplitude $|C_{n'}|$ with T, (b) phase shift $\phi(v_c, C_{n'})/\pi$ as a function of T.

small values of α, up to $\alpha = 0.5$. The variation of the phase shift ϕ between $v_c(x, z, t)$ and $C_{n'}$ according to α at the period $T = 0.5$, shows that the delay of response of the segregation to the velocity excitation, although increasing with α, seems globally not very sensitive to the variation of α and close to π, which corresponds to rather large phase shifts (Fig. 7(b)).

4.2.2. *Effect of the perturbation period*

In Figs. 8(a) and (b) we plot respectively the evolution of the amplitude and the phase shift of the normalized radial segregation $C_{n'}$ as a function of the period T of the convective velocity oscillations for the case $\alpha = 0.2$. We notice that $|C_{n'}|$ increases with T, reaches a maximum for a period T between 0.7 and 0.8 and then decreases slightly for larger periods (Fig. 8(a)). As for the phase shift between the velocity $v_c(x, z, t)$ and the segregation $C_{n'}$, Fig. 8(b) shows a decrease of the phase shift according to T, but the values remain large even for large periods. No theoretical model is available for comparison in this case.

4.3. *Illustration of the striations in the crystal*

Fig. 9 shows the solidified alloy structure for different cases of oscillation of v_c. We note that the composition field of the solid sample depends directly on the oscillation and we notice in particular that, in the case of an oscillation with a small period, the system has not enough time to adapt itself to the velocity variations, thus resulting in a structure very close to that corresponding to a solidification with a steady convective velocity.

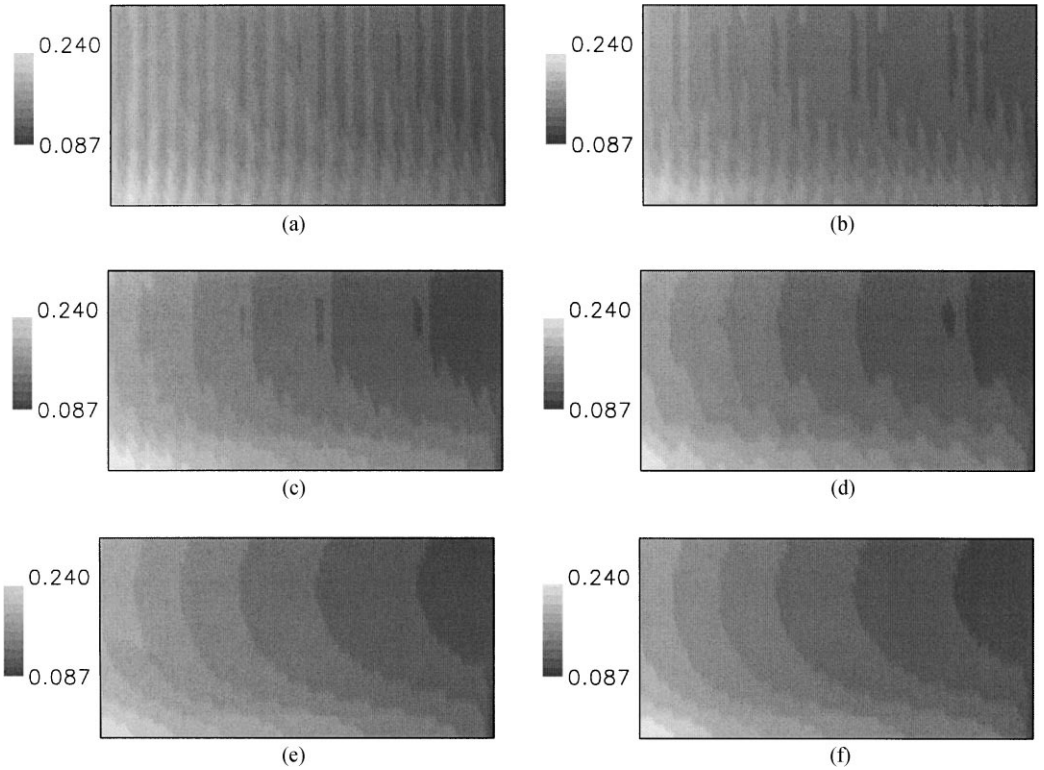

Fig. 9. Solute distribution in solidified alloy for different values of α and T: (a) $\alpha = 0.85, T = 0.5$, (b) $\alpha = 0.5, T = 0.5$, (c) $\alpha = 0.2, T = 0.5$, (d) $\alpha = 0.2, T = 1.0$, (e) $\alpha = 0.2, T = 0.1$, (f) non-oscillatory case.

4.4. Discussion

Using the identity $\delta = \Delta(D/V_1)$, the relation between the pulsation Ω of the analytical model (4) and the dimensionless period T of the numerical simulations can be written as

$$\Omega = \omega\delta^2/D = 2\pi \mathrm{ScPe}^{-2}\Delta^2 T^{-1}. \quad (8)$$

The non-dimensional numbers of Schmidt and Péclet are fixed in the present study, $\mathrm{Sc} = 10$ and $\mathrm{Pe} = 2$. The value of the convecto-diffusive parameter, deduced from the numerical results on macrosegregation [3], is also constant in the frame of this work, $\Delta = 0.2$. Using this value in Eqs. (5) and (6), we get $G_S = -0.18$ and $\Omega_C = 0.82$ as characteristics of the first-order filter given by the analytical model for longitudinal segregation. The cut-off non-dimensional period (T_C) is thus $T_C = 0.77$. The predictions of the analytical model in terms of amplitude and phase shift are given in Figs. 6(a) and (b), respectively, (with $G_S = -0.10$ not $G_S = -0.18$) along with the numerical results. Keeping in mind that there is no adjustable parameter in the model, the agreement can be considered as fairly good. The main difference concerns the phase shift at large periods.

Nevertheless, it should be noted that a much better agreement between numerical simulations and analytical solutions had been observed in the fluctuating interface velocity problem [6].

Regarding radial segregation, no analytical model is available for comparison with the numerical results. However, one can notice that the phase shift between the convection and composition fluctuations is much higher than for axial segregation. This can be qualitatively understood by the fact

that the spatial range of the concentration gradient is larger in the radial case (H versus δ). The time needed for a composition information to travel along the interface is thus necessarily higher. Regarding the comparison with the fluctuating interface problem, the phase shifts observed between excitation and response are here much higher which can be qualitatively understood by stating that interface velocity variations are directly felt at the growth front whereas convective variations are filtered through the solute boundary layer.

5. Concluding remarks

Our purpose in this work was to analyse in detail the effect of unsteady convection on solute incorporation. Numerical simulations of the mass transport phenomena in a horizontal Bridgman configuration were thus carried out. The imposed variations of the convection velocity covered a large amplitude and frequency range. The induced axial and radial segregations are often rather small, even at high perturbation amplitudes. The agreement of the numerical results with the predictions of a simplified analytical model based on the solutal boundary layer concept was found good. The present problem is one more example of the ability of the boundary layer model to efficiently capture the physics of transient solute transport phenomena.

To finish with, a point on the relevant frequency range is worth stating. As observed in the fluctuating interface velocity problem, in many actual growth configurations, the cut-off frequency Ω_C will be of order of magnitude unity (see Eq. (6)). In turn, this translates into a dimensional cut-off pulsation $\omega_c \cong D/\delta^2$ in the Hertz range, provided typical values such as $D = 10^{-8}\,m^2\,s^{-1}$ and $\delta = 10^{-4}\,m$ are used as inputs. It can thus be stated that high-frequency perturbations, e.g. associated with machinery operation, should then be significantly damped. On the other hand, at the low-frequency end of the spectrum, special care should be devoted to the optimization of the thermal regulation.

Acknowledgements

The present work has been conducted within the frame of the "Action de Recherche Amont" between the LMFA of "Ecole Centrale de Lyon" and the CEREM. The contribution of J.P. Garandet is part of the Gramme agreement between the CNES and the CEA.

References

[1] S. Kuppurao, S. Brandon, J.J. Derby, J. Crystal Growth 155 (1995) 103.
[2] T. Jung, G. Müller, J. Crystal Growth 165 (1996) 463.
[3] S. Kaddeche, H. Ben Hadid, D. Henry, J. Crystal Growth 135 (1994) 341.
[4] J.P. Garandet, J.J. Favier, D. Camel, in: D.T.J. Hurle (Ed.), Handbook of Crystal Growth, Vol. 2, North-Holland, Amsterdam, 1994, p. 659.
[5] J.R. Carruthers, A.F. Witt, in: R. Ueda, J.B. Mullin (Eds.), Crystal Growth and Characterization, North-Holland, Amsterdam, 1975.
[6] F.Z. Haddad, J.P. Garandet, D. Henry, H. Ben Hadid, J. Crystal Growth 204 (1999) 213.
[7] J.I.D. Alexander, J. Ouazzani, F. Rosenberger, J. Crystal Growth 97 (1989) 285.
[8] T. Jung, G. Müller, J. Crystal Growth 171 (1997) 373.
[9] J.P. Garandet, S. Corre, S. Gavoille, J.J. Favier, J.I.D. Alexander, J. Crystal Growth 165 (1996) 471.
[10] S. Corre, Ph.D. Thesis, INP-Grenoble, 1997.
[11] J.P. Garandet, J. Crystal Growth 131 (1993) 431.
[12] D.T.J. Hurle, E. Jakeman, E.R. Pike, J. Crystal Growth 3,4 (1968) 633.
[13] B. Roux (Ed.), GAMM Workshop: Numerical Simulation of Oscillatory Convection in Low-Pr Fluids, Notes on Numerical Fluid Mechanics 27, Vieweg, Braunschweig, 1990.
[14] J.F. Thompson, Z. Vawarsi, C.W. Mastin, Numerical Grid Generation, Elsevier, Amsterdam, 1985.
[15] R. Hirsh, J. Comput. Phys. 19 (1975) 90.
[16] J.J. Favier, Acta Met. 29 (1981) 197.
[17] J.P. Garandet, J. Crystal Growth 114 (1991) 593.